6

Soft capacitance fibers for touch-sensitive smart textiles

S. GORGUTSA and M. SKOROBOGATIY,
Ecole Polytechnique de Montréal, Canada

DOI: 10.1533/9780857093530.1.154

Abstract: We start with an overview of state-of-the-art tactile sensor technology. We then detail tactile sensors based on the novel soft capacitor fibers developed by our group and go on to introduce a theoretical model to describe the electrical response of a single capacitor fiber using an electrical ladder network model and show that such a fiber can function as a touch-sensitive sensor. Effects of different parameters on the sensing performance of a soft capacitor fiber are also studied. Finally we argue that capacitor fibers are ideally suited for wearable touch-sensing and as proof of this concept we present the prototype of a woven touchpad sensor featuring a one-dimensional array of capacitor fibers, and then study its performance.

Key words: flexible electronics, fibers, conducting polymers, sensors.

6.1 Introduction: overview of capacitive sensing

Touch sensing as a human interface device (HID) technology is becoming increasingly popular and ubiquitous, finding applications in smart phones, computers and responsive garments, to name a few. Various touch sensing systems have been developed based on different physical principles including resistive, capacitive, infrared, surface acoustic wave, electromagnetic, near field imaging, etc. Resistive (Cok *et al.*, 2004) and capacitive (Kalendra and Piazza, 1994) methods have been widely used in conventional touch screens of commercial products such as mobile phones, PDAs and consumer electronics devices. Resistive touch screens are composed of two material sheets that are coated with a resistive material, commonly indium tin oxide (ITO), and separated by an air gap or microdots. When a finger presses the screen, the two sheets are connected at the touch position, which changes the current flow in the screen. A sensing circuit then detects the changes and locates the touch position. A capacitive touch sensor is based on the capacitive coupling effect. A typical design involves coating the screen with a thin, transparent metallic layer, in order to form a collection of capacitors on the surface. Thus, when a user touches the surface, the disturbance caused by the finger changes the capacitance and current that flows on the display.

A significant limitation for most of these technologies is that they are only capable of detecting a single touch. Multi-touch techniques allow touch screens

to recognize touches of multiple fingers or inputs of multiple persons simultaneously. The multi-touch detection mechanisms can be classified into three categories: sensor array, capacitive sensing, and vision and optical-based ones. A sensor array touch surface consists of a grid of touch sensors that work independently. When a user exerts multiple touches on the surface, the system can identify activated sensors and determine these touch positions simultaneously. An example, originally proposed by Lee *et al.* (1985), is the Fast Multiple-Touch-Sensitive Input Device (FMTSID) – one of the first multi-point touch sensor-based devices. The system consists of a sensor matrix panel, rows of sensors, A/D converter and a control CPU. The design of the sensor matrix is based on the technique of capacitance measurement between a fingertip and a metal plate. A capacitive touch method uses the capacitive coupling between two conductors to sense a touch. Typically, the touch surface contains a mesh of horizontal and vertical antennas, which function as either a transmitter or a receiver of electric signals. Examples based on this technology include Rekimoto's SmartSkin (Rekimoto *et al.*, 2002) and DiamondTouch developed by Dietz and Leigh (2001).

In addition to touch screens, touch sensors with force-sensing abilities have been studied as tactile sensors for many years (Dahiya *et al.*, 2010). Such sensors have found their applications in artificial skin for robot applications (Engel *et al.*, 2003), minimally invasive surgery (Eltaib and Hewitt, 2003), wearable computers (Hoshi and Shimoda, 2006), and mobile or desktop haptic devices (Ruspini *et al.*, 1997). Up-to-date tactile sensors have mainly focused on silicon-based sensors that use piezoresistive (Beebe *et al.*, 1995; Wolffenbuttel and Regtien, 1991) or capacitive sensing mechanism (Chu *et al.*, 1995; Gray and Fearing, 1996; Leineweber *et al.*, 2000). The silicon tactile sensors have limitations of mechanical brittleness, and hence are not capable of sustaining large deformations. Polymer-based tactile sensing approaches that use piezoelectric polymer films (Dario and De Rossi, 1985; Kolesar *et al.*, 1996; Yuji *et al.*, 2006), pressure-conductive rubber (Shimojo *et al.*, 2004), carbon fiber-based polymer composite (Park *et al.*, 2009) and conductive polymers (Kim *et al.*, 2009) have also been reported. These sensors provide good spatial resolution but the applied force range is low due to the limited thickness of a membrane.

To integrate tactile sensors into the smart-textiles applications we could, for example, use arrays of conventional rigid electric devices embedded into a textile matrix, as was done in early prototypes of 'smart apparel'. However, this approach does not provide acceptable wearing comfort or good mechanical properties. This motivated recent efforts to develop truly wearable smart textiles. So far, capacitive sensing is probably the most promising technique for the textile-based sensors, as it does not depend on the applied mechanical force (including bends and stretching) and also enables multi-touch and gesture recognition functionality. In the next section, we will discuss novel all-polymer soft capacitor fibers recently developed by our research group and their applications in tactile sensing.

6.2 Soft capacitor fibers for electronic textiles

Recently there have been several reports on capacitor fibers compatible with a textile weaving process. By adding an external inductance, such fibers make a resonant LC circuit, thus allowing the use of many highly sensitive resonant detection techniques, which are able to detect small changes in the capacitor structure. Among several proposals for a capacitor fiber, we note a multicore fiber capacitor in the form of a bundle of approximately 50 μm-sized coaxial cables connected in parallel at a micro-level (Cheng and Hong, 2001). However, such capacitors were never actually fabricated. Load-bearing composite textiles comprising a large number of simple coaxial cables have been recently reported by the Air Force Research Laboratories (Baron *et al.*, 2006) for distributed storage of electrical energy directly in the fuselage of an airplane for pulsed weapons applications. The invention envisions reduction in the aircraft payload by combining mechanical and electric functionalities in the same fiber. Finally, the group of Baughman (Dalton *et al.*, 2003) proposed carbon nanotube-based textile threads that can be adapted to build super-capacitor textiles after soaking such threads in electrolyte.

Another novel type of electronic fiber was recently developed in our laboratory – high capacitance, soft fiber from conductive polymer composites. One key advantage of our fibers is that they do not require the use of electrolytes for their operation, which is especially desirable for wearable applications. Another key advantage is that the fibers can be made fully polymeric (no metallic electrodes) and very soft for applications in wearable sensing. Because of the relatively high capacitance of the fiber (60–100 nF/m), it can also be used for energy storage applications. In terms of capacitance, our fibers take an intermediate position between the coaxial cables and super-capacitors. Thus, capacitance of a coaxial cable with comparable parameters is typically 1000 times smaller than that of our fibers.

6.2.1 Fiber materials and fiber fabrication

Soft capacitor fibers are fabricated by the fiber drawing technique, which consists of three steps. The first step involves rolling or stacking conductive and dielectric films into a multilayer preform structure. During the second step, the preform is consolidated by heating it to temperatures somewhat above the polymer glass transition temperature (T_g). Consolidation is needed as the diffusion of the polymer molecules through interfaces of adjacent layers fuses these layers together, thus reducing the effect of property mismatch of different materials in the drawing process. Finally, at the third step, consolidated preform is drawn into fibers using a fiber drawing tower. Drawing is typically performed at temperatures higher than the polymer T_g. During successful drawing, the resultant fibers generally preserve the structured profile of a preform, thus fibers with complex microstructures can be fabricated via homologous reduction (during drawing) of

a macrostructure of the preform. The described drawing technique is directly analogous to the one used in manufacturing microstructured polymer optical fibers (Gao *et al.*, 2006).

Flexible multilayer capacitors discussed in this chapter generally consist of two conducting polymer layers serving as two electrodes of a capacitor, and two isolating polymer separator layers. To draw successfully, the preform materials should be compatible with each other in terms of their rheological and thermo-mechanical properties. In our first tests, we have attempted drawing a thin continuous layer of low-melting temperature metal sandwiched between two isolating polymer layers. As a metal we have used Bi_{58}/Sn_{42} alloy with a melting point of 138°C. Various polymers were tested as isolating layers. However, we found that in all cases it was difficult to preserve the laminated structure with a thin metal foil during the drawing process. Particularly, when melted, metal foil would break into wires during drawing, thus destroying the continuous electrode structure. We have rationalized this observation by noting that the visco-elasticity, ductility and interfacial tension of alloy and the surrounding polymer cannot match well at drawing temperatures. For example, at the temperature for the polymer to be drawn into fibers, the viscosity of melted metal becomes very low, thus it is easy for a thin sheet of melted metal to develop flow instability and form several larger wires to minimize surface energy associated with a polymer/metal interface.

Another potential problem during drawing of metal sheets is that when the polymer surrounding the molten metal becomes too soft, it can no longer hold the melt; as a consequence, a large drop of metal would form at the preform end, even before drawing starts, thus draining the rest of the preform from the metal. From these initial experiments we have concluded that drawing of a thin metallic sheet sandwiched between two plastic sheets is in general problematic due to a strong mismatch of the material properties during the drawing process.

After realizing the challenge of drawing metallic electrodes in the form of thin sheets, a natural option to remedy this problem was to substitute metals with thermoplastic conductive polymers as electrodes. Unfortunately, thermoplastic intrinsic conductive polymers suitable for drawing are not available commercially. The only thermoplastic conductive polymers that are currently available commercially are either carbon black (CB) filled or most recently carbon nanotube filled films. In our research we have mostly used polyethylene(PE)-based CB-filled films (BPQ series) provided by Bystat International Inc. The film, with a thickness of 91 μm, has a surface resistivity of 17 KΩ/sq. The measured volume resistivity is around 2.2 Ωm along the surface. To find the isolating materials that can be co-drawn with this conductive film, we have tried various polymer films, such as polyvinylidene fluoride (PVDF), polycarbonate (PC), polyethylene terephthalate (PET), polymethyl methacrylate (PMMA), and others. Among all the attempted polymers, we have found that the two best materials for the isolating layer are low density polyethylene (LDPE) film or a PC film.

6.2.2 Capacitor fiber designs

We have developed three distinct fiber capacitor geometries that will be discussed in this chapter. They all share the same concept, but each of them possesses its own features. The first fiber type has a cylindrical geometry with two plastic electrodes in the form of a spiraling multilayer (Fig. 6.1(a)). The central part of a fiber was either left empty with the inner plastic electrode lining up with the hollow core, a metallic electrode was introduced into the hollow core during drawing, or the core was collapsed completely thus forming a plastic central electrode. In all these fibers, the second electrode was wrapped around the fiber. The second fiber type (Fig. 6.1(b)) is also of cylindrical multilayer geometry; however, it features two hollow cores lined with two plastic electrodes. The fiber is wrapped into an isolating material, so there is no direct contact with the environment. During drawing, two metallic electrodes were introduced into the

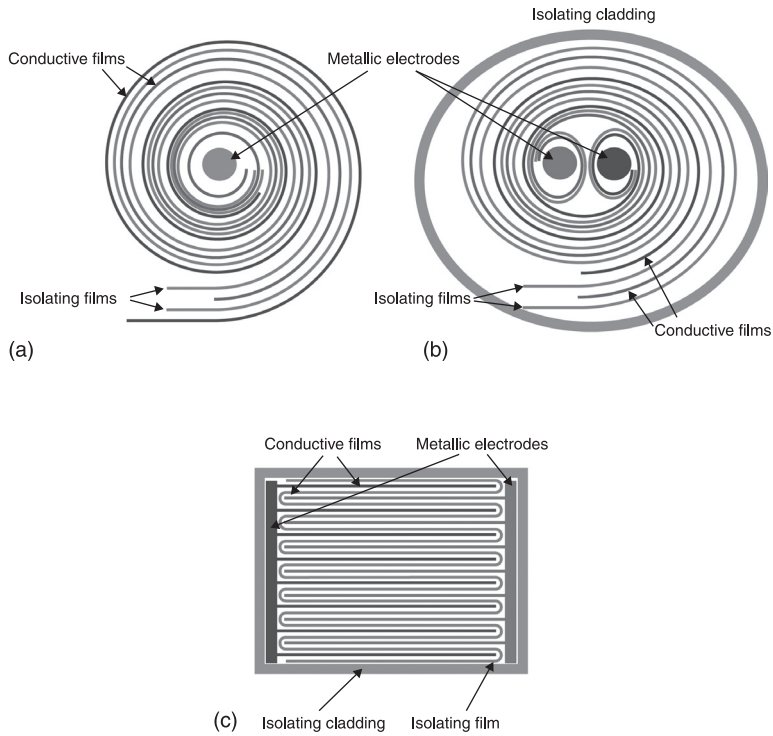

6.1 (a) Schematic of a cylindrical capacitor fiber preform featuring a spiraling multilayer comprising two conductive and two isolating films. (b) Schematic of a cylindrical capacitor fiber with two electrodes in the center. (c) Schematic of a rectangular preform prepared by encapsulating a zigzagging stack of two conductive and an isolating layer inside a rectangular PMMA tube.

fiber cores. Finally, the third fiber type features a square electrically isolating tube comprising a zigzagging stack of plastic electrodes (Fig. 6.1(c)) separated by a zigzagging dielectric layer. The metallic electrodes were integrated on the left and right sides of a tube for ease of connection.

Fibers of the first type (Fig. 6.1(a)) were fabricated by co-rolling the two conductive polymer films, which were physically and electrically separated with the two isolating LDPE films. In the resultant fiber, the inner conductive film forms one electrode inside the hollow fiber core, while another electrode is created by the other conductive film at the fiber surface. A similar fabrication strategy was used in the second fiber type (Fig. 6.1(b)), with the only exception being the positioning of two isolated fiber cores in the fiber center, while encapsulating the fiber into an isolating HDPE plastic wrap. Finally, fibers of the third type (Fig. 6.1(c)) were created by encapsulating a zigzagging stack of the electrodes and isolating layers inside a rectangular PMMA tube.

6.2.3 Capacitor fiber connection and potential applications

An important issue, when designing any smart fiber, concerns connection of such fibers either to each other or with the external electrical probes. In view of various potential applications of a capacitor fiber, we have explored several connection geometries. In Figs. 6.2(a–e), we show four complete designs for a capacitor fiber. In each figure we present both the structure of a preform before drawing, as well as the structure of a resultant fiber.

Design one is presented in Figs. 6.2(a) and (b), where we show a circular hollow core fiber with the first electrode formed by the conductive layer lining the hollow fiber core (Fig. 6.1(a)), and the second electrode formed by the other conductive layer wrapping the fiber from outside. The outside electrode is exposed for ease of access. The hollow core can be either collapsed (Fig. 6.2(b)) or left open during drawing (Fig. 6.2(a)). In general, to access the electrode inside the fiber core, we have to use a needle-like electrical probe; in fact, we have used 50 to 100 μm diameter hypodermic needles to perform electrical characterization of this fiber. One of the advantages of the hollow core fibers is that they are very soft due to lack of metallic components in their structure and, therefore, are most suitable for integration into wearable textiles. Moreover, the hollow fiber core can be filled with functional liquids, which will be in direct contact with one of the electrodes. This can be useful for various sensing applications, where physical or chemical properties of a liquid could be interrogated electrically.

Design two is presented in Fig. 6.2(c), where we show a circular hollow core fiber with one of the electrodes formed by a small 100 μm diameter copper wire, which is integrated into the fiber core directly during drawing. With a tension-adjustable reel installed on the top of a preform, the copper wire can be passed through the preform core, pulled down and embedded into the fiber center during drawing by collapsing

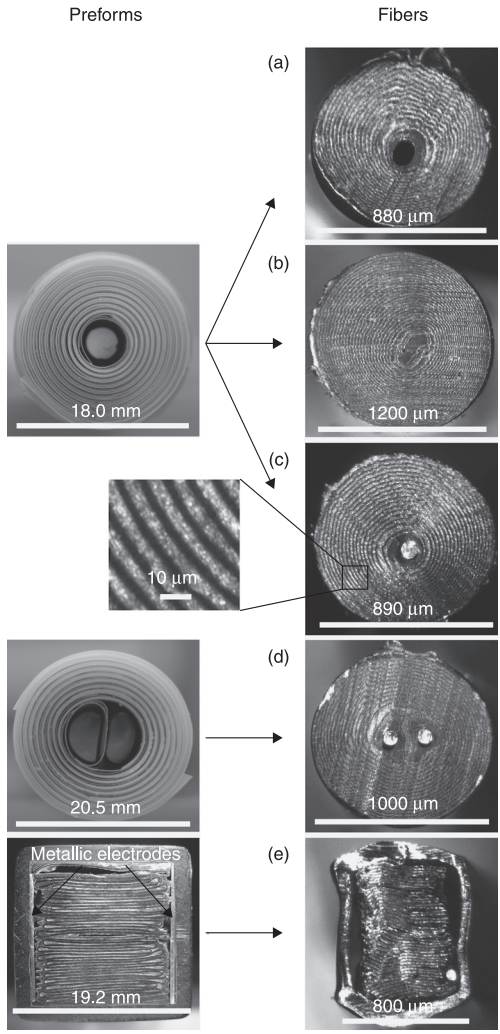

6.2 Design I: hollow core fiber with the first electrode lining the inside of a hollow core, and the second plastic electrode wrapping the fiber from outside. During drawing, fiber hollow core can be left open (a) or collapsed (b), depending on the application requirement. Design II: Hollow core fiber can be drawn with a metallic electrode in the center. Such an electrode can be a copper wire (c) in contact with the plastic electrode lining the hollow core. Design III: fiber containing two hollow cores. The cores are lined with two plastic electrodes electrically separated from each other. Fiber is drawn with two copper wires threaded through the hollow cores in the preform (d). Design IV: square fiber capacitor. Fiber features a zigzagging stack of two plastic electrodes separated with an electrically isolating PC layer (e). Also two metallic electrodes are placed in contact with plastic electrodes, and the whole multilayer is encapsulated inside a square PMMA tube.

plastic cladding around it. The second electrode is formed by the other conductive layer wrapping the fiber from outside, similar to the first design. The main advantage of this design is the ease of connection to the inner electrode, as the plastic capacitor multilayer can be easily stripped from the copper wire. This fiber has lower effective resistivity compared to the hollow core fiber, as one of the electrodes is made of a highly conductive metal. Despite the copper electrode in its structure, the fiber is still highly flexible. As the outside electrode is exposed, this fiber can be used for the detection of electromagnetic influence or as a proximity sensor.

Design three is presented in Fig. 6.2(d), where we show a circular fiber containing two hollow cores positioned in the middle of the fiber. Each core is lined with distinct conductive layers, which are forming electrodes one and two. The cores with electrodes are electrically isolated from each other. Moreover, the whole preform is then wrapped into several layers of pure LDPE plastic to isolate the capacitor layers from the environment. The preform is then drawn with two copper wires threaded through its holes. The resultant fiber features two copper electrodes and a fully encapsulated capacitor multilayer. Such fibers can be interesting for energy storage applications, due to ease of connection and electrical isolation from the environment.

Finally, design four is presented in Fig. 6.2(e), where we show a thin PMMA tube of square cross section, comprising a zigzagging multilayer of the two conductive layers separated by a single electrically-isolating PC layer. The first plastic electrode is located to the left and the second plastic electrode is located to the right of the isolating PC layer. At the left and right inner sides of the square tube, we place foils of Bi_{58}/Sn_{42} alloy in contact with the plastic conductive layers. During fiber drawing, wire-like metallic electrodes are created from the foils.

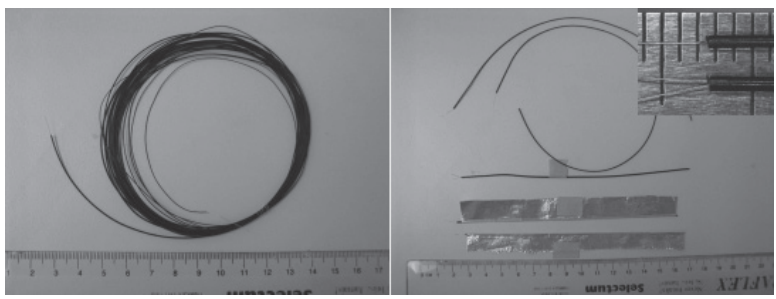

(a) (b)

6.3 (a) Capacitor fiber fabricated from the preform shown in Fig. 6.2(c). The fiber features a central 100 μm-thick copper wire, as well as an exposed conductive plastic electrode on the fiber surface. (b) To perform electrical characterization of the fibers, embedded copper wire is used as the first electrical probe, while the second electrical probe is an aluminium foil wrapped around the fiber conductive surface. The inset is an enlarged view of the fibers with single and double copper wire electrodes.

Finally, the structure of the resultant fiber is similar to the one of an encapsulated fiber with two copper electrodes.

In comparison with standard capacitors, we notice that a 10 nF ceramic capacitor measures about 600 × 300 μm and 10 μF components measure 2.0 × 1.25 mm. The fiber capacitor does not possess advantages over the standard capacitors in terms of size, but the flexibility and softness it features are essential for applications in wearable smart textiles. Encapsulation of RC series in a single fiber makes the circuit in wearable e-textiles more compact and reliable, because it may reduce the number of connection joints. Although the equivalent resistance of the capacitor is very high for a short fiber, which is limited by the properties of available conductive films, it can be reduced simply by increasing the length of the fiber, as demonstrated in the following.

6.3 Electrical characterization of the isolated capacitor fiber

To characterize electrical properties of our capacitor fibers, we used the measurement circuit presented in Fig. 6.4, where the fiber capacitor is connected to a function generator (GFG-8216A, Good Will Instrument Co., Ltd) through the reference resistor R_{ref} = 480 kΩ. The function generator provides a sinusoidal signal of tunable frequency ω = (0.3 Hz to 3 MHz). An oscilloscope (GDS-1022, Good Will Instrument Co., Ltd) measures the input voltage V_{Ch1} (ω) on channel 1 and the output voltage over the reference resistor V_{Ch2} (ω) on channel 2. A 10X probe (GTP-060A-4, Good Will Instrument Co., Ltd) was used to acquire the experimental data. The voltage produced by the function generator is fixed and in the whole frequency range of interest equals to V_{Ch1} = 2 V. In our experiments, we

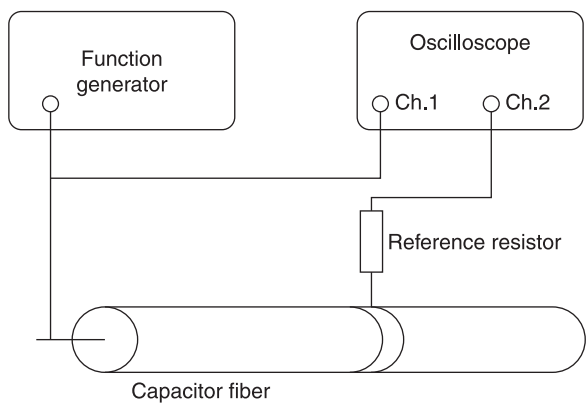

6.4 Schematic of a measurement set-up.

measured both the amplitudes and the phase difference between channels 1 and 2. Due to high resistivity of our fibers, and also to fit the experimental data at higher frequencies ($\omega > 1$ kHz), we have to take into account the effective impedances of an oscilloscope.

In this section, we present the properties of fiber capacitance and resistance as a function of various fiber geometrical parameters. Most of the presented measurements were performed on fibers featuring a single copper electrode in their cores, while the second electrode was formed by the plastic conductive layer on the fiber surface (Fig. 6.2(c)). The fiber was co-drawn with a 100 μm-thick copper wire in its center. In the preform, both conductive layers are 75 μm thick, while the two insulating layers are made of 86 μm thick LDPE films. To characterize capacitance fibers, we used embedded copper wire as the first electrical probe, while the second electrical probe was made by wrapping aluminum foil around a part or the whole of the fiber (Fig. 6.3).

6.3.1 RC ladder network model of a soft capacitor fiber fully covered with a foil probe

The high resistivity of conductive composite films endows the capacitor fiber with a distributed response. In particular, the fiber electrical properties can be well-described by an RC ladder circuit. First, we consider the case when the fiber outer electrode is fully covered with a highly conductive foil probe. In this case, the problem becomes two-dimensional (2-D) (no longitudinal currents) and the RC ladder circuit presented in Fig. 6.5 describes transverse currents in the capacitor cross section.

In Fig. 6.5, a schematic of the ladder model is presented, where R_t corresponds to the transverse resistance of a single conductive film spiraling from the fiber

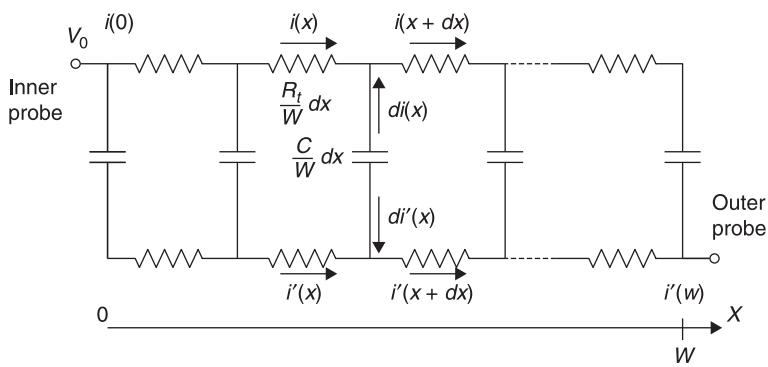

6.5 Ladder network model of the capacitor fiber fully covered with a foil probe.

core towards its surface. The value of the transverse resistance can then be approximated as:

$$R_t \approx \rho_v \frac{W}{Ld_c} \quad [6.1]$$

where ρ_v is the volume resistivity of the conductive films, L is the length of the fiber, and W and d_c denote, respectively, the width and thickness of the conductive electrodes wrapped in the fiber cross section (Fig. 6.2). To measure transverse resistance, we have to ensure that there are no longitudinal (along the fiber length) currents in the fiber. In practice, to deduce transverse resistance, we cover the outer fiber electrode (high resistance electrode) with a metallic foil, and then measure fiber AC response by applying the voltage between the inner copper electrode and the outer metallic foil.

For the longitudinal currents, fiber resistance will be:

$$R_l \approx \rho_v \frac{L}{Wd_c} \quad [6.2]$$

which for longer samples ($L > W$) is much higher than the transverse resistance. To measure the longitudinal resistance, we have to ensure that there are no transverse (perpendicular to the fiber length) currents in the fiber. In practice, it is difficult to measure the longitudinal resistance directly. In principle, if the electrode length (fiber length) is much longer than the net width of a conductive electrode wrapped in the fiber cross section, longitudinal resistance can be deduced from the AC measurement, where the high resistance outer electrode of a fiber is grounded at one end, while the inner high resistance electrode of the fiber is connected to a voltage supply at the other. Note that the low resistance copper electrode has to be removed from the fiber for this measurement and DC measurements are not possible, as in the described configuration, the fiber acts as a capacitor. Clearly, when connecting to a fiber using a continuous probe (i.e. foil) along the whole fiber length, fiber resistance will be dominated by its transverse component.

Another fundamental parameter that determines fiber performance is the fiber capacitance, denoted as C in Fig. 6.5. As thicknesses of the dielectric and conductive layers in the fiber are hundreds of times smaller than the fiber diameter, fiber capacitance can be approximated using an expression for the equivalent parallel-plate capacitor:

$$C \approx 2\varepsilon_0 \varepsilon \frac{WL}{d_i} \quad [6.3]$$

where ε is dielectric constant of the isolating films, ε_0 is permeability of the vacuum, and d_i is thickness of the rolled isolating films.

As shown in Fig. 6.5, $i(x)$ and $i'(x)$ denote the current flowing in the conductive film connected to the inner probe and outer probe, respectively. V_0 is the voltage

difference between the inner probe and outer probe. We assume that the resistivity of the conductive film is a position-independent and frequency-independent parameter. Appling Kirchhoff's Voltage Law (KVL) and Kirchhoff's Current Law (KCL) to the ladder circuit, leads to the following equations:

$$\int_0^x \frac{R_t}{W} i(l)\,dl + \frac{W}{j\omega C}\frac{di'(x)}{dx} + \int_x^W \frac{R_t}{W} i'(l)\,dl = V_0 \qquad [6.4]$$

and

$$di(x) = -di'(x) \qquad [6.5]$$

with boundary conditions:

$$i(0) = i'(W) \text{ and } i'(W) = 0. \qquad [6.6]$$

Equations 6.4 to 6.6 can be solved analytically, and yield the following expressions for the effective transversal capacitance and effective transversal series resistance:

$$C_F(\omega) = -\frac{1}{\omega R_t \cdot Im\Big(f(B)\Big)} \qquad [6.7]$$

$$R_F(\omega) = \frac{R_t}{2} + R_t \cdot Re\Big(f(B)\Big) \qquad [6.8]$$

where

$$f(B) = \frac{1+\cosh(B)}{B\cdot\sinh(B)}; \quad B = \sqrt{2j\omega R_t C}. \qquad [6.9]$$

Note at low frequencies, such as $B \rightarrow 0$, Eqs. 6.7 and 6.8 reduce to the frequency-independent values as:

$$C_F = C, R_F = \frac{2}{3} R_t. \qquad [6.10]$$

6.3.2 Frequency dependent response of the capacitor fibers

As predicted by Eqs. 6.7 and 6.8, effective capacitance and effective resistance of the capacitor fibers are dependent on the operational frequency, with limiting values at low frequencies given by Eq. 6.10. In this section, we present results of experimental studies of the frequency dependent response of the capacitor fibers. To interpret correctly the measured response $V_{Ch2}(\omega)$ of the electric circuit, it is important to consider the complex impedance of the oscilloscope and the electric probe used in the characterization. This is mainly due to the relatively large

resistance of our fibers. We must also be aware that conductive films used in the fiber fabrication can show significant frequency-dependence of their electrical properties. For example, it has been reported (Nakamura and Sawa, 1998) that near the percolation threshold, the resistivity of CB/polymer films decreases with increasing frequency. To find the effective circuit parameters of an oscilloscope, we first measured the response of a known resistor having a similar resistance to that of a fiber (~477 kΩ). We noted that complex impedance of the measuring circuit (oscilloscope) becomes important only at frequencies higher than 100 kHz. We then studied the frequency response of the conductive film, and found that its resistivity is frequency independent below 300 kHz. Therefore, in all the experiments that followed, we have operating frequencies lower than 100 kHz.

In Fig. 6.6, we present experimentally measured frequency dependent fiber resistance and capacitance of a fiber fully covered with a foil probe and with diameter of 0.93 mm and length of 137 mm. At low frequencies, both C_F and R_F are virtually constants, while they decrease at frequencies higher than 1 kHz. This behavior is similar to that of a standard electrolytic capacitor and can be well-explained by the RC ladder network model with a characteristic response frequency of $1/(R_tC)$~4 kHz. We can also see that Eqs. 6.7 and 6.8 provide good predictions of the experimental data, by assuming $C = 9.4$ nF and $R_t = 26$ kΩ in the model.

6.3.3 Effect of the capacitor fiber length

In order to study dependence of the fiber properties as a function of the fiber length, we have used two fiber samples of different lengths that were drawn from

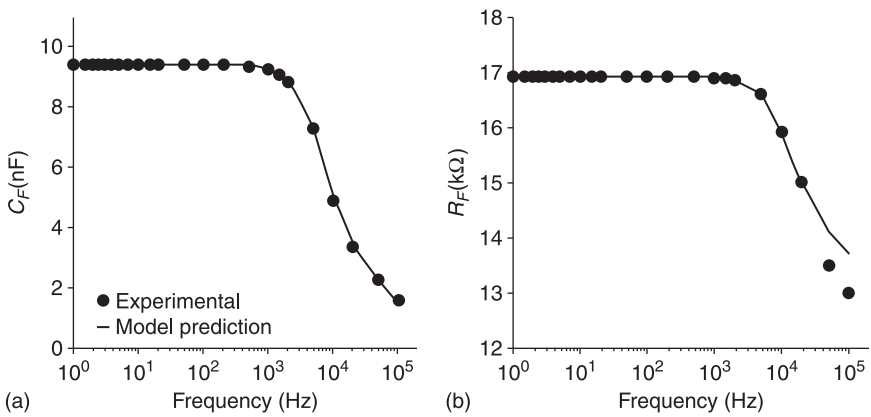

6.6 Comparison of experimental data and model predictions of frequency responses of a fiber capacitor. (a) Effective capacitance versus frequency. (b) Effective resistance versus frequency.

the same preform. Sample #1 and sample #2 had outer diameters of 920 to 980 μm and 720 to 760 μm, respectively. Both samples were drawn from the same preform at speeds around 100 mm/min at 180°C. The two samples were then cut into sections of different lengths ranging between 10 and 60 cm, and then wrapped with aluminum foil with 100% coverage ratio. The experiments were conducted at low frequencies (ω <1 kHz), so that effective capacitance and resistance can be considered as constant. In Fig. 6.7a, we present measured fiber capacitance as a function of fiber length and observe a clear linear dependence. From this data, we see that for all the fibers the capacitance per unit length is around 69 nF/m (inset in Fig. 6.7(a)), which is very close to the value of 69.5 nF/m measured for the capacitance of the fiber preform. This is easy to rationalize from Eqs. 6.3 and 6.10. As W/d_i is constant during drawing (because of the largely homologous drawing), hence C_F/L should be the same for any fiber produced from the same preform, regardless of the fiber size. The reason why our fibers can obtain large capacitance is because the value of W/d_i is much larger than that of a coaxial cable with one capacitive layer. In contrast, fiber resistance decreases inversely proportional to the fiber length. In fact, it is rather the product $R_F \cdot L$ that is approximately constant, as shown in the inset of Fig. 6.7(b). Equations 6.1 and 6.10 indicate that if ρ_v is constant, $R_F \cdot L$ should also be a constant, because W/d_c is the same for fibers drawn from the same preform. However, we also find that the thinner fiber shows a larger value of $R_F \cdot L$. This diameter dependency is implied in the volume resistivity ρ_v in Eq. 6.1. It is reported that the resistivity of CB/polymer

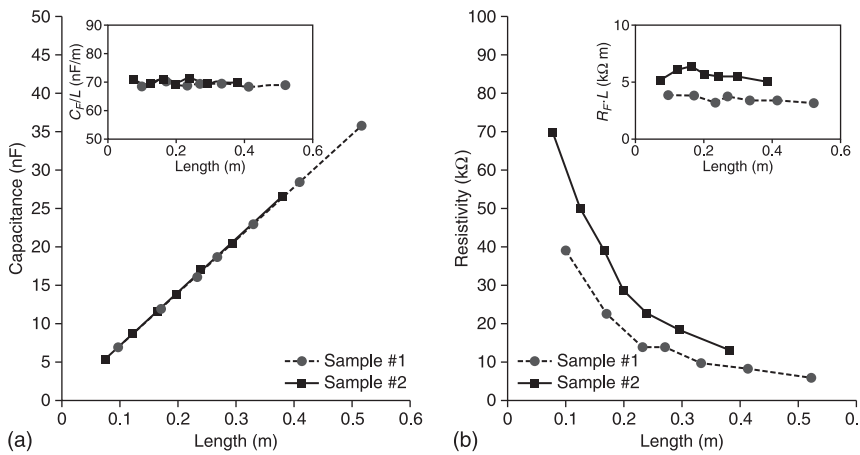

6.7 Dependence of: (a) fiber capacitance and (b) fiber resistivity on fiber length. Two data sets denoted by square and round points correspond to the two fiber samples of different diameters drawn from the same preform. Insets: dependence of the (a) fiber capacitance per unit length C_F/L and (b) fiber resistivity factor $R_F \cdot L$ on the fiber length.

composites increase as the material is stretched, and the value is proportional to the elongation ratio in logarithm scale (Schulte *et al.*, 1988; Feng and Chan, 2003). Thus, we observed that the thinner fiber has a larger $R_F \cdot L$ value.

6.3.4 Effect of the operation temperature on the fiber's electrical properties

The effect of the temperature of operation on the electrical properties of a capacitor fiber is presented in Fig. 6.8. Sample #1 was 135 mm long and had a diameter of 840 μm, while sample #2 was 133 mm long and had a diameter of 930 μm. To control the temperature of the two samples, they were fixed on top of a hot plate. Our measurements at low frequencies show that fiber capacitance per unit length remains almost independent of the temperature of operation, while fiber resistivity increases rapidly as the temperature rises. This result is in good correspondence with the recent reports on positive temperature coefficient (Tang *et al.*, 1997; Yu *et al.*, 1998) for the resistivity of the composites of CB and LDPE in the 0 to 100°C temperature range. The effect of thermal expansion and a consequent increase of the average distance between CB particles are thought to be the main reasons for the positive temperature coefficient of the conductive polymer composites. This interesting property promises various applications of capacitor fibers in self-controlled or self-limiting textiles responsive to temperature or heat.

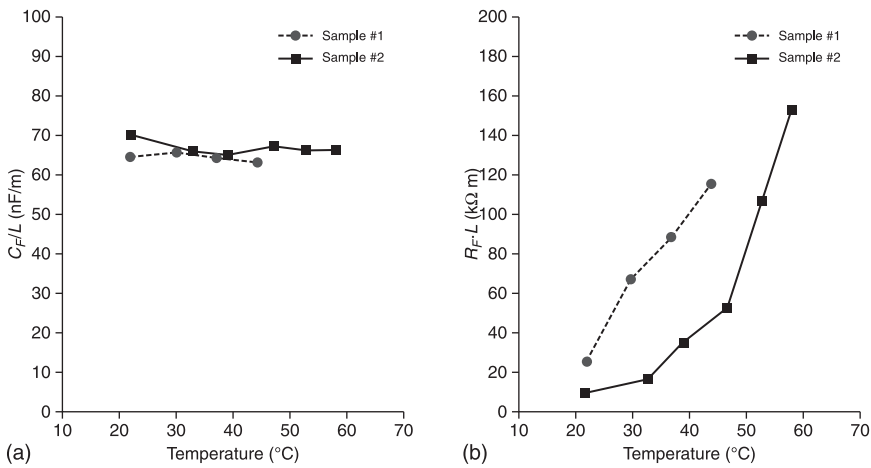

6.8 Effect of the temperature of operation on electrical properties of a capacitor fiber. (a) Capacitance per unit of length C_F/L. (b) Resistivity factor $R_F \cdot L$. Sample #1 has a diameter of 840 μm and a length of 135 mm. Sample #2 has a diameter of 930 μm and a length of 136 mm.

6.3.5 Effect of the fiber drawing parameters

Electrical performance of the capacitor fibers is equally affected by the fiber geometrical parameters and by the fiber material parameters. In this section, we show that fiber fabrication parameters, such as fiber drawing temperature and fiber drawing speed, can have a significant effect on the fiber resistivity, while also somewhat affecting the fiber capacitance. Generally, capacitor fibers presented in this work can be drawn at temperatures in the range of 170 to 185°C, with drawing speeds ranging from 100 to 300 mm/min.

Generally, we find that the fiber capacitance C_F/L is largely independent of the fiber diameter and drawing parameters, and equals to that measured directly in the fiber preform. In contrast, fiber resistivity parameter $R_F \cdot L$ is significantly affected by the drawing parameters. From Eqs. 6.1, 6.3 and 6.10, we can relate fiber capacitance per unit length and fiber resistivity parameters as:

$$\frac{R_F L}{C_F/L} \propto \frac{\rho_v}{\varepsilon_0 \varepsilon} \qquad [6.11]$$

While fiber capacitance is indeed almost independent of the fiber geometrical and processing parameters, fiber resistivity is strongly influenced by them. This can be rationalized by concluding that bulk resistivity of the CB polymer composite can change significantly during the drawing procedure from its original value in the fiber preform. To further validate our observation that drawing at lower temperatures results in higher resistivities, we performed a set of stretching experiments at room temperature on the planar conductive films. It was found that the resistivity of the conductive film increases as much as by two orders of magnitude from its original value when the films were stretched unheated to about twice their length. Similar observation has been reported in the literature for CB-filled polymers and polymer composites (Schulte *et al.*, 1988; Feng and Chan, 2003).

Conclusions of these experiments can be rationalized as follows. During the drawing process, the conductive polymer composite in the preform undergoes various processing stages including heating, melting, stretching, annealing and cooling. The stretching increases the distance between the individual CB particles in the stretching direction, thus disrupting the conductive network. During the annealing above glass transition temperature, CB particles aggregate together through Brownian motion and form a continuous network. The destruction and reconstruction of the conductive network is highly dependent on the concentration and properties of CB and processing parameters such as mixing strength, temperature and time and the annealing temperature and time, etc. (Wu *et al.*, 2000; Zhang *et al.*, 2007). If the fiber is drawn at a lower temperature and higher speed, the stronger viscous stress of the polymer matrix may disintegrate CB particles and decrease their aspect ratio, thus making the conductive network more difficult to form. The annealing conditions have a direct influence on the formation

of the conductive network (Wu *et al.* 2000). The rising of the annealing temperature decreases the viscosity of the matrix polymer, thus facilitating the movement and aggregation of the CB particles. This, in turn, reduces the time needed for the CB particles to build up a conductive network. It is well-reported that the resistivity of polymer composites filled with CB (Wu *et al.*, 2000; Cao *et al.*, 2009) or carbon nanotube (Alig *et al.*, 2008), decreases as the annealing temperature and time increase. This explains our experimental observation about lower drawing speeds resulting in lower fiber resistivities; this is because a lower drawing speed leads to a longer annealing time in the furnace. In addition, a lower drawing speed corresponds to a weaker stretching and slower deformation. This not only avoids CB particles being disintegrated, but also provides them with more time to create a conductive network before cooling down to room temperature.

6.4 Capacitor fiber as a one-dimensional distributed touch sensor

In this section, we study properties of the individual soft capacitor fiber as a one-dimensional (1-D) tactile sensor integrated into the textile base. To ease the integration and connection of the fibers, a small-diameter (typically 50–150 μm) copper wire was embedded into the fiber during the drawing process by passing it inside of the fiber preform (Fig. 6.9) central hole and letting the preform collapse around the wire in the neckdown region. For the reader unfamiliar with fiber drawing procedure, we would like to explain that the neckdown region is a 'transitional' region between the preform and the resulting fiber, where the preform converges to the size of the resulting fiber. Introduction of a copper wire into the fiber drawing process actually improves the fiber drawability. In this configuration, copper wire in the fiber center serves as a low resistivity electrode attached to one of the two high resistivity conductive plastic electrodes of a fiber capacitor. The other high resistivity conductive plastic electrode of a fiber is brought to the fiber surface to ease connection. Typical fibers fabricated using the above-mentioned fabrication procedure have a sub-millimeter diameter, contain at least 30 layers, and have a typical capacitance of 100 nF/m, which is almost three orders of magnitude higher than that of a standard coaxial cable of comparable diameter.

High resistivity of the conductive polymer electrodes together with high capacitance endows the fiber with interesting electrical properties, which as we will see below, makes the fiber well suited for distributed sensing applications of touch. In a typical implementation of a touch sensor, we ground the outer fiber electrode (high Ω electrode in Fig. 6.9) on one end, while applying the AC voltage to the copper wire (low Ω electrode in Fig. 6.9) on the other end (Fig. 6.10). We then read out the voltage on the fiber outer electrode (high Ω electrode) at the same end where the copper wire is connected. In our experiments, we found that the read-out voltage is highly sensitive to the position of the touch along the fiber.

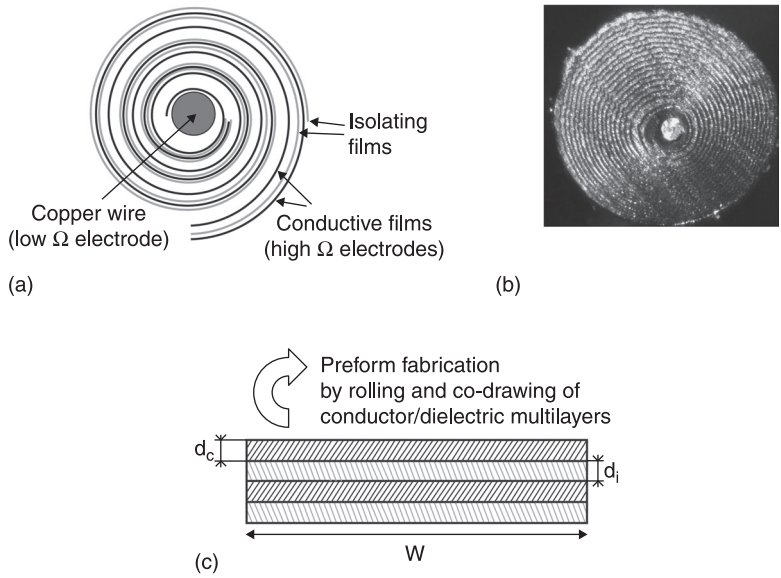

6.9 (a) Schematic of a capacitor fiber featuring a spiraling multilayer comprising two conductive and two isolating films. Black curves represent two conductive films, while grey curves represent isolating films. (b) Photo of the cross-section of a drawn capacitor fiber with a cooper wire embedded in the center. (c) Fiber preform is made by co-rolling four polymer layers (2 conductive and 2 isolating) into a Swiss roll structure. The number of resultant layers in a spiral structure is proportional to the width of the unrolled multilayer. In the drawn fiber, thicknesses of the conductive d_c and isolating d_i layers can be smaller than 10 μm, while the unwrapped width W of the layers fitting into a 1 mm diameter fiber can be in excess of 3 cm.

In the following we describe basic principles behind touch sensing using a single capacitor fiber and then consider a theoretical model that describes capacitor fiber response to the touch.

6.4.1 Electrical response of a single capacitor fiber

To characterize a single fiber, we use the general electrical layout outlined earlier. In particular, a sinusoidal signal of voltage amplitude V_0 and constant frequency (10 Hz–10 kHz) is provided by an external function generator and is applied to the copper wire electrode of a fiber (Fig. 6.10). Voltage response is acquired using a sliding contact on the outer electrode of a fiber (high Ω electrode). The sliding contact is connected to the oscilloscope as before through a 10X probe. This arrangement allows measuring the voltage distribution along the fiber length, both when the fiber is touched or not. As a human body is largely composed of conductive electrolytes covered with a layer of dielectric skin, the human body

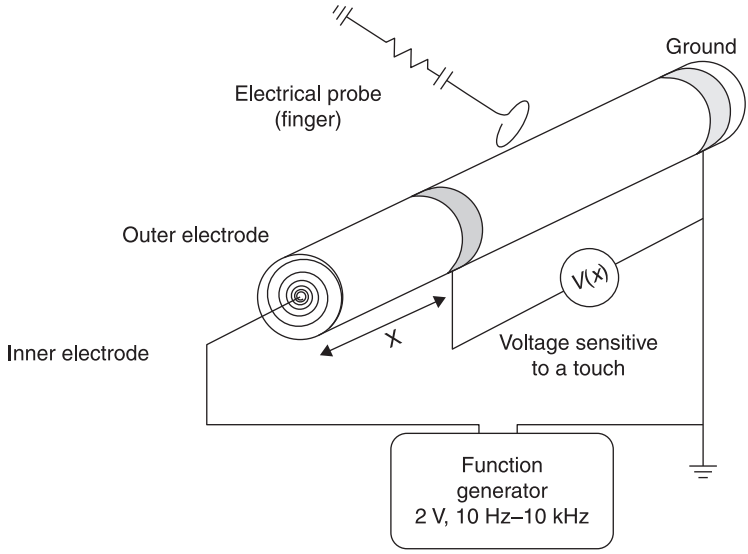

6.10 Schematic of a one-dimensional slide sensor based on a single capacitor fiber.

can be approximated with an equivalent electrical circuit comprising a resistor connected in series to a capacitor. Typical values of an effective resistance and capacitance are 1.44 kΩ and 150 pF, respectively. In our experimental studies of a single fiber response to touch, we use an equivalent human probe with these effective electrical parameters to guarantee repeatability between measurements and to simplify theoretical interpretation of the acquired data.

In Fig. 6.11, we present voltage distribution along the fiber length for an isolated fiber (Fig. 6.11(a)), and for the fiber that is touched with an equivalent human probe (Fig. 6.11(b)). Here x/L represents the normalized position of a sliding contact along the fiber length. The fiber length used in our experiments was L = 12.3 cm. $|V(x)/V_0|$ represents the voltage measured by the sliding contact along the outer electrode of a capacitor fiber. When using an equivalent human probe (Fig. 6.11(b)), we fix it at position x/L = 0.3. Different data sets in Fig. 6.11 correspond to the four different frequencies of a function generator used in our measurements (10 Hz, 100 Hz, 1 kHz, 10 kHz).

In the DC case (not shown in the figures), voltage along the outer electrode of a capacitor is constant and zero, as the outer high-resistive electrode provides a DC-connection to ground. For an isolated fiber (Fig. 6.11(a)) in the AC case, voltage distribution along the fiber length shows the same trend at all frequencies. In particular, it saturates exponentially fast from zero at the grounded end to some maximal value at the other end of the fiber.

From Fig. 6.11(b), it is clear that when operating at higher driving frequencies, the touch position can be determined from the dip in the voltage distribution along

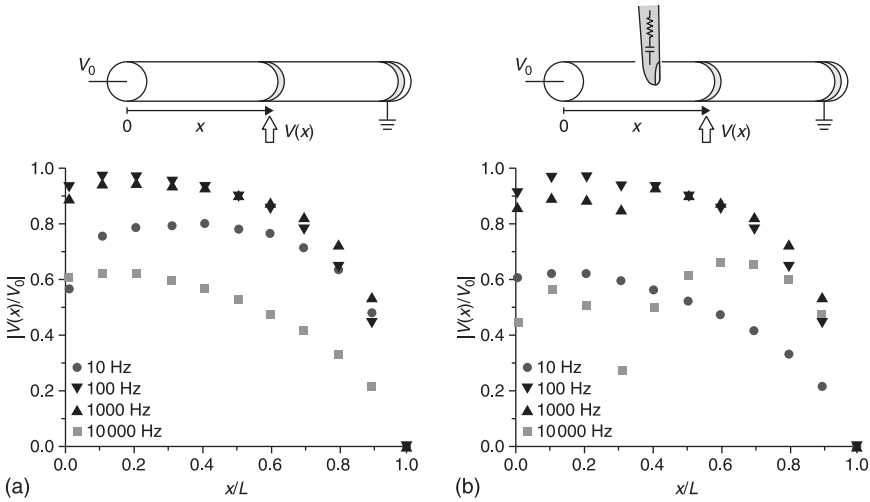

6.11 Voltage distribution along the outer fiber electrode for: (a) an isolated fiber; and (b) a fiber touched with an equivalent human probe. Four data sets correspond to the different driving frequencies of 10 Hz, 100 Hz, 1 kHz and 10 kHz. Voltage distribution along the fiber touched with a probe shows a dip in the vicinity of a touching position.

the fiber outer electrode. For practical implementation of a slide sensor, it is, however, inconvenient to require knowledge of the voltage distribution across the whole fiber length. Therefore, the important question is whether position of touch can be determined by continuously measuring the voltage at a single fixed point on the fiber outer electrode. To answer this question, in Fig. 6.12, we present the value of voltage as measured at the fiber extremity ($x = 0$) as a function of the touch position along the fiber. Now x/L represents the touch position of the equivalent human probe, while $|V(0)/V_0|$ represents the voltage measured at the fiber end opposite to the grounded end. We observe that for driving frequencies above 100 Hz, the voltage at the fiber extremity changes significantly, depending on the position of touch. In turn, this allows building a 1-D sliding sensor with a convenient acquisition procedure based on a single point measurement.

6.4.2 RC ladder network model for the capacitor fiber featuring one highly conductive, and one highly resistive, electrode

To model electrical response of the capacitor fibers, we start with the RC ladder network presented in Section 6.3 and first consider a stand-alone capacitor fiber without touching. As before (Eqs. 6.1 and 6.2), we define the conductive

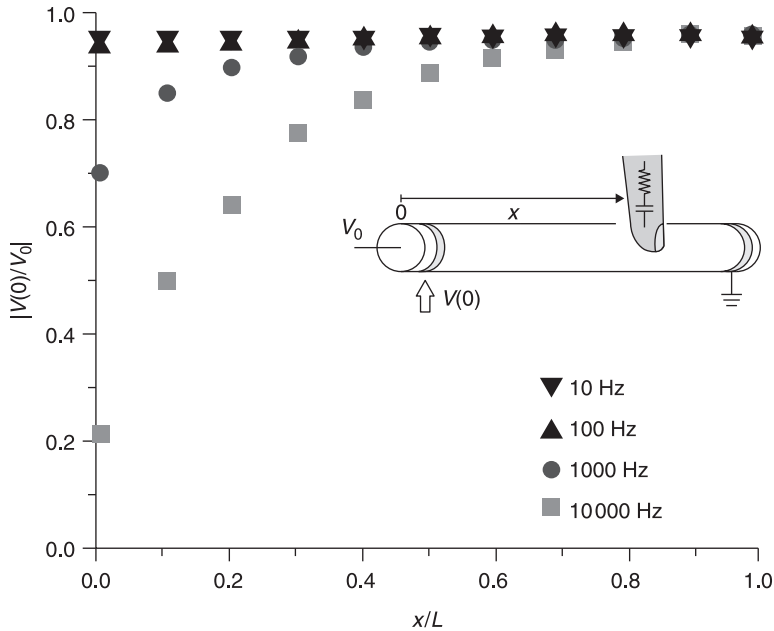

6.12 Voltage measured at the extremity of a capacitor fiber opposite to the fiber grounded end.

polymer electrode transverse resistance as $R_t \approx r_t/L$, where the electrode resistivity is $r_t = \rho_v W/d_c$. Longitudinal resistance is given by $R_l \approx r_l/L$, where $r_l = \rho_v/(Wd_c)$ is the electrode longitudinal resistivity. Finally, the total fiber capacitance is proportional to the fiber length, while the fiber capacitance per unit length is simply $C_t \approx 2\varepsilon_0 \varepsilon W/d_i$ (Eq. 6.3), where d_i is the thickness of the isolating films in the fiber, ε is the dielectric constant of the isolating films, and ε_0 is permeability of the vacuum.

We note that relatively high capacitance of our fibers is due to the small thickness of the isolating films, and large net width of the conductive layers. Thus, a typical fiber features conductive and isolating layers with thicknesses smaller than 10 μm, while the net width W of the layers wrapped into a 1 mm diameter fiber can be in excess of 3 cm.

Now let us consider a capacitor fiber as a sequence of thin cross sections of length dx (Fig. 6.13(a)), each having a longitudinal resistance $dR_l = r_l dx$ for the outer (surface) electrode. We then consider electrical response of an individual cross section, while assuming that along the fiber length the individual fiber sections are connected via longitudinal resistance elements dR_l (Fig. 6.13b). Electrical response of an individual fiber cross section is modeled as an RC network, where transverse resistance elements $dR_t = r_t/dx$ are connected via capacitance $dC_t = C_t dx$ elements. In Section 6.3, we have shown an equivalent

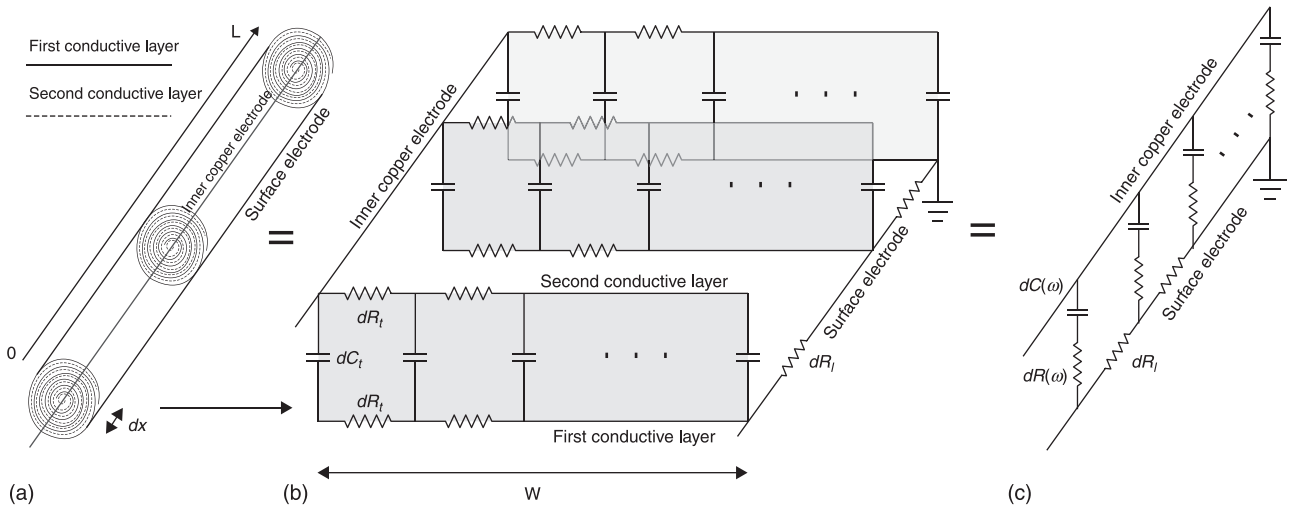

6.13 Ladder RC network model of a stand-alone capacitor fiber. (a) The fiber is modeled as a sequence of fiber cross sections of small length *dx* connected in series via longitudinal resistive elements (high resistivity outer electrode), while assuming that the inner copper electrode has a constant potential along its length. (b) Electrical response of an individual fiber cross section is modeled as an RC network, where transverse resistivity elements are connected via capacitance elements. (c) Also the scheme above corresponds to the longitudinal resistance element, which is the frequency dependent resistance and capacitance of an individual fiber cross section of length *dx*. It could be shown that an equivalent circuit that describes electrical response of an individual fiber cross section is given simply by the frequency dependent resistivity connected in series with frequency-dependent capacitance. Finally, the electrical response of a fiber is modeled as another RC network with frequency-dependent resistivity and capacitance.

circuit that describes electrical response of an individual fiber cross section of length dx is given by the frequency dependent resistance $dR(\omega)$ connected in series, with frequency dependent capacitance $dC(\omega)$, where:

$$dC(\omega) = -\frac{dx}{\omega r_t \cdot \mathrm{Im}\left(f(B)\right)}, \quad [6.12]$$

$$dR(\omega) = \left(\frac{1}{2} + \mathrm{Re}\left(f(B)\right)\right)\frac{r_t}{dx}, \quad [6.13]$$

and

$$f(B) = \frac{1+\cosh(B)}{B\cdot\sinh(B)};\ B = \sqrt{2j\omega\cdot r_t C_t}. \quad [6.14]$$

Electrical response of a stand-alone fiber can, therefore, be modeled as another RC ladder with frequency-dependent $dR(\omega)$, $dC(\omega)$, and frequency-independent parameters dR_l (Fig. 6.13(c)).

Now that the model for a stand-alone capacitor fiber is defined, we modify it slightly in order to analyse a 1-D slide sensor. In particular, the fiber is assumed to be touched at a position x_b with a finger having effective electric parameters R_b = 1.44 kΩ, C_b = 150 pF. Moreover, to simplify comparison with the experiment, we include in our model the effective circuit of an oscilloscope probe used in our measurements. The probe is attached at a position x_p on the fiber surface (Fig. 6.14), and the effective circuit parameters of a probe and oscilloscope are R_p = 10 MΩ, C_p = 200 pF. The necessity to include effective circuit of a probe into the model comes from the realization that resistance of a standard 10X probe (10 MΩ) used in our experiments has the same order of magnitude as the transverse resistance of the short fiber segments used in our studies. For example, transverse resistance of the 10 cm-long fiber pieces typically ranges in 0.1 to 1 MΩ. Moreover, we can show that at frequencies lower than $v \approx 1/(2\pi R_p C_b) \approx 100\,Hz$ or higher than $v \approx 1/(2\pi R_b C_p) \approx 55\,kHz$, the effective impedance of a probe becomes smaller than that of a finger, therefore the probe effective circuit has to be included in the model to accurately explain experimental measurements.

In Fig. 6.14, we distinguish three parts of an RC ladder network. The first part is located to the left of the probe, where $i''(x)$ denotes the longitudinal current flowing in the polymer conductive film, while $di''(x)$ denotes the transverse current flowing in the thin section of length dx. To the right of the probe, while still before the finger touch position, the longitudinal and transverse currents in the polymer electrode are denoted as $i(x)$ and $di(x)$. Finally, to the right of the touch position, the corresponding currents are $i'(x)$ and $di'(x)$. V_0 is the voltage difference between the inner copper electrode and the outer electrode at $x = L$. We also assume that the fiber material parameters are position and frequency independent. Furthermore, we consider that the probe is attached to the left of touch position $x_p < x_b$. We now apply the KVL and KCL to the ladder circuit to

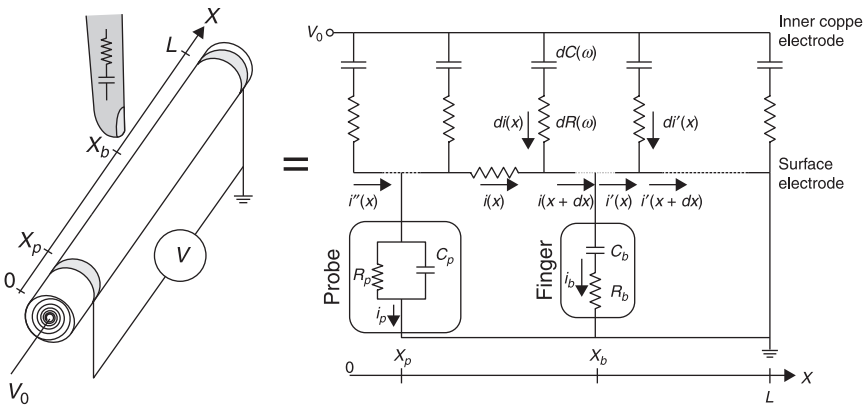

6.14 The ladder network model of a one-dimensional slide sensor. The fiber is assumed to be touched at a position x_b with a finger having effective electric parameters R_b, C_b. Moreover, to simplify comparison with experiment, we include in our model the effective circuit (with parameters R_p, C_p) of an oscilloscope probe used in our measurements; the probe is attached at a position x_p.

arrive at the following equations for any position x along the fiber. Thus, using KVL, we get:

$$
\begin{aligned}
&0 < x < x_p \quad ; \quad di''(x)\left(\frac{1}{j\omega\, dC(\omega)} + dR(\omega)\right) + \int_x^{x_p} r_l\, i''(l)\, dl = V_0 - V\left(x_p\right)\\
&x = x_p \quad ; \quad i_p \frac{R_p}{1 + j\omega C_p R_p} = V\left(x_p\right)\\
&x_p < x < x_b \quad ; \quad di(x)\left(\frac{1}{j\omega\, dC(\omega)} + dR(\omega)\right) + \int_x^{x_b} r_l\, i(l)\, dl = V_0 - V\left(x_b\right)\\
&x = x_b \quad ; \quad i_b\left(\frac{1}{j\omega\, C_b} + R_b\right) = V\left(x_b\right)\\
&x_b < x < L \quad ; \quad di'(x)\left(\frac{1}{j\omega\, dC(\omega)} + dR(\omega)\right) + \int_x^{L} r_l\, i'(l)\, dl = V_0.
\end{aligned}
\qquad [6.15]
$$

Using the KCL, we get:

$$
\begin{aligned}
&0 < x < x_p \quad ; \quad i''(x) + di''(x) = i''(x + dx)\\
&x = x_p \quad ; \quad i''(x_p) = i(x_p) + i_p\\
&x_p < x < x_b \quad ; \quad i(x) + di(x) = i(x + dx)\\
&x = x_b \quad ; \quad i(x_b) = i'(x_b) + i_b\\
&x_p < x < L \quad ; \quad i'(x) + di'(x) = i'(x + dx).
\end{aligned}
\qquad [6.16]
$$

Finally, the boundary conditions are:

$$i''(0) = 0. \qquad [6.17]$$

To solve these equations, we can first differentiate Eqs. 6.15 with respect to x to obtain three similar second-order differential equations with respect to i, i' or i'' in the following form:

$$\frac{d^2 i(x)}{dx^2}\left(\frac{1}{j\omega dC(\omega)/dx} + dx \cdot dR(\omega)\right) - r_l i(x) = 0. \qquad [6.18]$$

Then, in each of the three sections of the fiber, we can write a solution for the currents as:

$$i = C_1 e^{\tilde{B}x} + C_2 e^{-\tilde{B}x} \quad ; \quad i' = C_3 e^{\tilde{B}x} + C_4 e^{-\tilde{B}x} \quad ; \quad i'' = C_5 e^{\tilde{B}x} + C_6 e^{-\tilde{B}x} \quad [6.19]$$

where

$$\tilde{B} = \sqrt{\frac{r_l}{\left(\frac{1}{j\omega\, dC(\omega)/dx} + dx \cdot dR(\omega)\right)}} = \sqrt{\frac{r_l}{r_t\left(\frac{1}{2} + f(B)\right)}} \qquad [6.20]$$

and B, $f(B)$ are defined in Eqs. 6.12 and 6.13. Insertion of Eq. 6.19 into the remaining Eqs. 6.15 to 6.17 results in a set of linear equations from which the constants, C_1–C_6, can be determined. Finally, from the known current distributions, voltage distribution in the given position x measured from the surface electrode can be easily found as:

$$V(x) = V_0 - \frac{d^2 i(x)}{dx^2}\left(\frac{1}{j\omega\, dC(\omega)/dx} + dx \cdot dR(\omega)\right) \qquad [6.21]$$

Comparison of experimental data with predictions of a theoretical model

In Fig. 6.15 we present experimental data and the theoretical RC ladder model Eqs. 6.15 to 6.21 prediction for the dependence of voltage measured at $x_p = 0$ as a function of the equivalent human probe touch position x_b. In each graph, different sets of curves correspond to distinct fibers, which are different from each other in a single parameter. Thus, in Fig. 6.15(a), we present measurements of three fibers drawn using preforms containing different number of conductive layers, and as a consequence, having different capacitance C. The preforms were drawn using the same temperature profile and drawing speed so as to guarantee similar values of the bulk resistivity of the polymer electrodes. Then, the fiber geometrical parameters, such as layer thicknesses, electrode width and

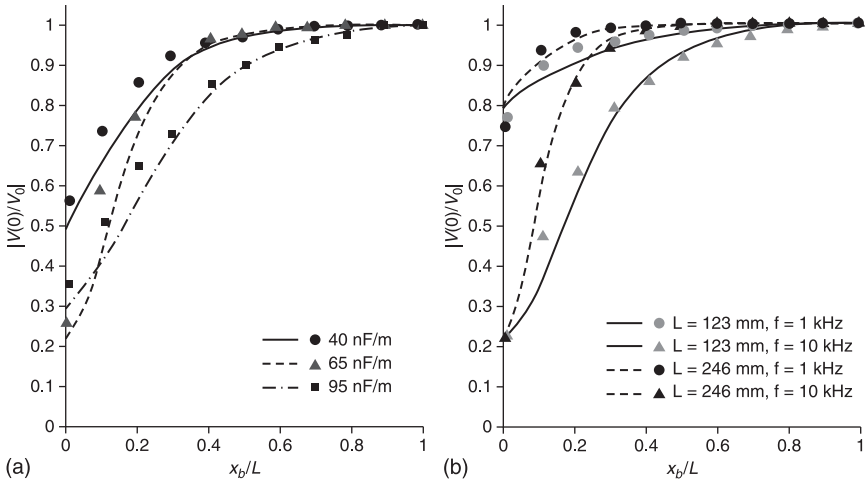

6.15 Fiber response to the touch of the equivalent human probe – comparison between predictions of the RC ladder model and experimental data. (a) Response at 10 kHz of the 3 distinct fibers of the same length and different capacitances $C_t = 40\,\text{nF.m}^{-1}$, $C_t = 65\,\text{nF.m}^{-1}$, $C_t = 95\,\text{nF.m}^{-1}$. The rest of the geometrical and electrical parameters of the fibers are similar to each other. (b) Response at 1 and 10 kHz of the two distinct fibers of the different lengths. The rest of the geometrical and electrical parameters of the fibers are identical to each other, as a shorter fiber was obtained by cutting a longer fiber in half.

fiber length, were measured using the optical microscope. Parameters of the oscilloscope effective circuit were measured independently. Finally, bulk resistance of the conductive layers in a fiber was measured, as described in Section 6.3, by wrapping the fiber outer electrode in foil and then extracting the transverse resistance and, consequently, the bulk resistance of conductive layers from the fiber AC response. In this arrangement, the currents are purely transverse and the RC ladder model was shown (Section 6.3) to give precise fits for the bulk resistivity parameter. We then use all the model parameters found in the independent measurements to predict the response of the fiber to the touch. From Fig. 6.15(a) we see that at the operating frequency of 10 kHz, the experimental curves are well described by the RC ladder model, which does not use any fitting parameter.

Similarly, in Fig. 6.15(b), we present fiber response to the touch for two identical fibers of different lengths. In these experiments we first use the fiber of length 24.6 cm and then cut it in half to 12.3 cm and repeat the measurement. The rest of the input parameters necessary for the use of a theoretical model were measured as described above. From the figure, we see that fiber response is well described by the RC ladder model, both at 1 and 10 kHz operating frequencies.

Moreover, we see that this particular fiber becomes insensitive to touch if the touch point x_b is further than 10 cm from the measuring point x_p.

The measurement of fiber response as a function of fiber length, presented in Fig. 6.15(b), brings about an important question about the maximal length of a 1-D slide sensor, and about the optimal frequency of operation. We note that the functional form of the currents (Eq. 6.19) flowing between the probe and the measurement point is exponential with the characteristic length:

$$\tilde{L} = \frac{1}{\mathrm{Re}(\tilde{B})} = \frac{W}{\sqrt{2}} \frac{1}{\mathrm{Re}\left(\left(1+2f(B)\right)^{-\frac{1}{2}}\right)} \qquad [6.22]$$

where we used $\sqrt{r_t / r_l} = W$ – the total width of the rolled electrodes. We now use asymptotic expansions of the function $f(B)$:

$$f(B) = \frac{1+\cosh(B)}{B \cdot \sinh(B)} \underset{B=\sqrt{2j\omega \cdot r_t C_t}}{=} \begin{cases} \frac{1}{B} & ; \quad \omega >> \frac{1}{r_t C_t} \\ \frac{2}{B^2} & ; \quad \omega << \frac{1}{r_t C_t} \end{cases} \qquad [6.23]$$

to obtain the following limiting values for the characteristic length of the current decay:

$$\tilde{L} = \frac{W}{\sqrt{2}} \begin{cases} 1 & ; \quad \omega >> \frac{1}{r_t C_t} \\ \frac{1}{\sqrt{\omega r_t C_t}} & ; \quad \omega << \frac{1}{r_t C_t} \end{cases} . \qquad [6.24]$$

Note that for the slide sensor of length L to be sensitive along its whole length, we have to require that $L \sim \tilde{L}$. From Eq. 6.24, it means that at high frequencies $\omega >> 1/(r_t C_t)$ the maximal sensor length is limited by the net width of a polymer electrode wrapped into the fiber cross section. Note that for most of our fibers, the region of high frequency is in the vicinity or above 1 kHz. Furthermore, in a typical fiber of $D = 1$ mm diameter, we can currently fit $N \sim 10$ to 50 turns of the conductive electrode, which results in the net width of a conductive electrode in the fiber $W \sim \pi DN \sim 3$ cm–15 cm. Therefore, for the operation frequencies in the vicinity or above 1 kHz, the maximal length of the capacitor fiber-based slide sensor is currently limited to several tens of centimeters.

In principle, operating at lower frequencies allows match of the fiber length and characteristic current decay length $L \sim \tilde{L}$ for any desired length of the fiber. However, this demands very low operation frequencies of $\omega \sim (W/L)^2/(r_t C_t)$, which even for a relatively short 1 m-long fiber can be as low as 1 to 10 Hz. However,

operation at low frequencies is prone to strong electrical interferences and noise. Moreover, at low frequencies of ~1 Hz, the finger has very large impedance, >> 1 MΩ, which is mismatched with that of our fiber. This makes the sensor of very low sensitivity at low frequencies.

6.4.3 Interpreting electrical data from a single-fiber touch sensor

Finally, a 1-D slide sensor was characterized in a realistic setting with a student touching the sensor consecutively at different positions along the fiber length. At this time the sensor was touched with an actual finger and not an equivalent probe. The driving frequency was 1 kHz and was provided by the analogue output of an ADC card. The same card was also employed as a signal acquisition unit with an acquisition rate of 20 kHz. Such high acquisition rates were only used for the purpose of resolving the time response of a sensor and in practice significantly slower acquisition rates (<10 Hz) could be used. To deduce the touch position, we continuously measured the voltage at the endpoint of the fiber outer electrode. Figure 6.15(b) presents an example of the measured voltage as a function of time. To operate the sensor, we first record for several seconds the voltage level ('idle' level) without touching the fiber (see Fig. 6.16). We then

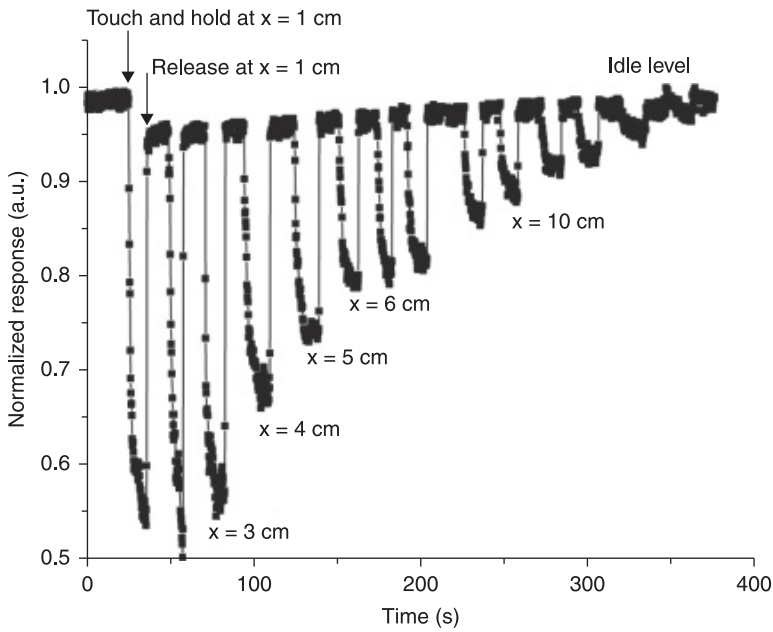

6.16 Typical time resolved response of a one-dimensional slide sensor. Dips in the measured voltage correspond to the touch and release events.

touch the sensor at $x = 1\,cm$ from the fiber end. At the moment of touch, the signal drops very fast (in a matter of 1 s) to almost its equilibrium value, and this is followed by a much slower (~10 s) relaxation to the actual equilibrium value. We believe that the fast timescale corresponds to a pure electrical response of a fiber, while the slow timescale corresponds to small pressure induced changes in the fiber electrical parameter due to fiber deformation under touch. As soon as the finger is removed, the signal returns back to the 'idle' level in a matter of 0.2 s. Next, by touching, holding and releasing the fiber at various positions along its length, we can record a complete calibration curve. Then the position of touch can be determined from the voltage level at the bottom of dips corresponding to touching events. This is, of course, the simplest implementation of a touch sensor. To avoid person-dependent calibration of the sensor, we can, for example, perform two voltage measurements from opposing sides of a fiber (by simultaneously flipping the ground from one side to the other), then use analytical models to extract the effective electrical parameters of a human figure and find the touch position.

6.4.4 Effect of the fiber length on sensitivity

To study the effect of fiber length on its sensing performance, we take two pieces of fiber, named sample #1 and sample #2, from the same batch of drawing. Sample #1, with a length of 123 mm, is a part of sample #2, with a length of 246 mm. Thus, they share the same electrical and geometric parameters. The samples have an equal diameter of around 1.1 mm. The geometric parameters, such as the thickness and width of films (d_c, d_i and W), can be measured from microscopic observations or calculated from the preform geometry and draw-down ratio. The fiber's electrical parameters were characterized independently by the method reported in Wu *et al.* (2000). The measured capacitance per unit length for both fibers equals 93 nF m^{-1}. The volume resistivity of the conductive film, calculated from transverse resistivity r_t, equals 4.5 Ωm. Figure 6.15(b) also shows a comparison of the experimental data and model predictions for samples #1 and #2 at frequencies of 1 and 10 kHz. The data below 100 Hz are not displayed, because the disturbance caused by finger touch at these frequencies is very small.

We can see that both fibers exhibit a voltage drop at the left end, which becomes more prominent as frequency goes higher. This phenomenon is precisely predicted by the model. In order to find the reasons that cause this observation, we made calculations using a model without the oscilloscope in the circuit, or simply set the value of C_p extremely small and the value of R_p extremely higher in the present model. The results show that if we neglect the effect of the oscilloscope, the voltage becomes a constant without any drop when the measurement point approaches the left end of the fiber. This implies that this voltage drop on this end of the fiber is rather caused by the decreased impedance of the oscilloscope at higher frequencies than by the fiber itself. From Fig. 6.15(b) we can also see that

the longer fiber, denoted by the grey color, has a longer part in the middle with its voltage be a constant, while the short fiber, denoted by the black color, has more part of its length with a changing voltage. This can be rationalized by the distributed nature of the fiber. The edge effect becomes more dominant when the fiber length decreases. In Fig. 6.15(b), we compare the effect of frequency on the fiber performance. For both fibers, the overall voltage decreases as frequency increases, which is related to the capacitance and resistance of the fiber.

6.4.5 Effect of the operational frequency on sensitivity

The maximal voltage amplitude at the outer fiber electrode is strongly dependent on the operation frequency and reaches its maximum at frequencies between 100 Hz and 1 kHz. When the fiber is touched with an equivalent human probe, voltage distribution along the fiber outer electrode shows high sensitivity to the operation frequency (Figs 6.9(a,b)). Thus, at low driving frequencies (10 Hz, 100 Hz), voltage distribution along the fiber outer electrode is virtually unchanged by the touch. At higher frequencies (>100 Hz), a dip appears in the voltage distribution in the vicinity of the point of contact with an equivalent human probe. Finally, at high frequencies (>1 kHz), this dip becomes very pronounced and easy to detect. Overall frequency response of the capacitor fiber can be understood from the basic electric circuit theory. Thus, the fiber used in these experiments had capacitance per unit length of C_t = 93 nF/m and transverse resistance per unit length of R_t = 14.5 kΩ·m (bulk resistance per unit length of conductive layers 4.8 Ω·m). The characteristic frequency associated with a corresponding RC circuit is $v = 1/(2\pi R_t C_t) = 120\,Hz$. Electric response of a capacitor fiber is, in fact, that of a high pass filter. Namely, at frequencies well below 120 Hz, the fiber operates in a quasi-DC regime, where it simply breaks the electrical circuit. Fiber response to touch is, therefore, minimal at low frequencies. At frequencies comparable or higher than 120 Hz, the capacitor fiber acts as s distributed complex impedance with relatively low resistance. At these higher frequencies, touching the capacitor fiber can modify significantly the local current flows and voltage distributions, thus resulting in sensitivity of its various electrical parameters to touching.

6.5 Fully woven two-dimensional touch pad sensor using one-dimensional array of capacitance fibers

6.5.1 Sensor design and fabrication

Soft but highly elastic mechanical nature of fibers makes them easy to use in conventional weaving process (Fig. 6.17(b)). In our laboratory we have used a table Dobby loom (Leclerc Voyager 15¾″ inch 4 s) to weave the fibers into a wool-based textile matrix (Fig. 6.17(b)). The resulting 15 × 10 cm woven touch pad contained 15 capacitor fibers, each 12 cm long (Fig. 6.17(c)).

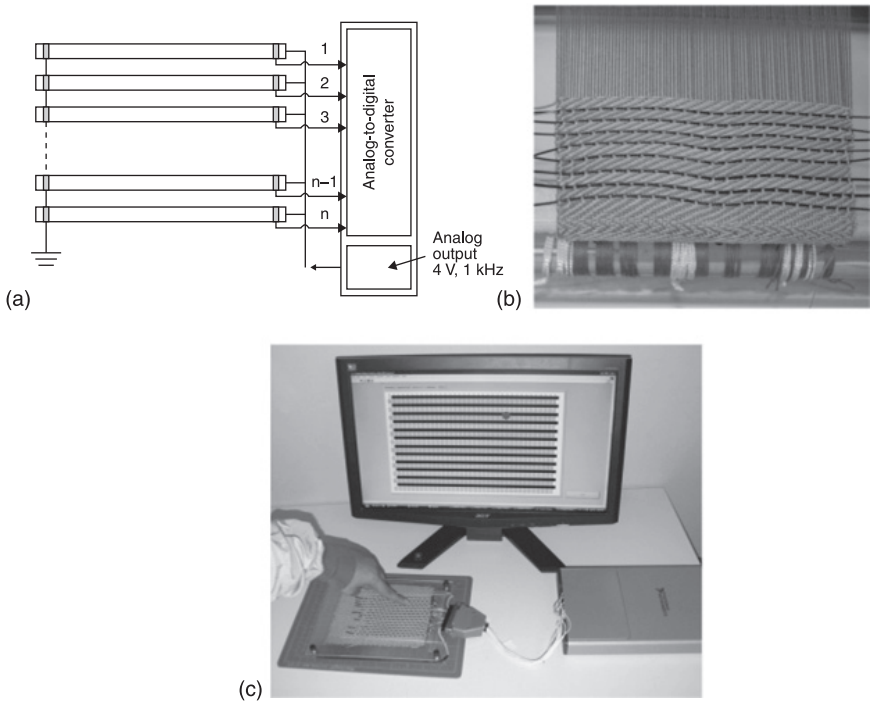

6.17 The woven touch pad sensor. (a) Schematic representation of the woven two-dimensional touch pad sensor featuring a one-dimensional array of the capacitor fibers. All the connections to and from the fibers are done using a 120 μm-diameter copper wire. Fibers in the array have the common ground and a common source; however, they are interrogated individually. Analog output of the ADC board is used as a function generator that provides a sinusoidal signal at 1 kHz with an amplitude of 4 V. (b) Weaving a two-dimensional touch pad sensor on a Dobby loom. (c) Woven touch pad connected to the ADC board, as well as the monitor image of a textile with an interpreted touch position.

In our experimental set-up, we use the same connection as described earlier: the inner (low Ω) electrodes of all the fibers (copper wires) are connected to the analogue voltage source integrated into the Analog-to-Digital Convertor (ADC) card, providing a sinusoidal signal at 1 kHz with amplitude of 4 V (Fig. 6.17(b)). The outer (high Ω) electrodes of the fibers are connected to the individual channels of the ADC card (National Instruments USB-6343 X-series DAQ), in order to measure the voltage at their endpoints. The connections are made using thin cooper wires (0.120 μm-diameter) and secured with a conductive epoxy.

We have already shown in Section 6.4 that the readout voltage measured at the end of the individual fiber is highly sensitive to the position of the touch along this fiber, which in this case acts like a tactile slide sensor. Thus, a 1-D senor array

integrated into the textile allows us to build a touch pad sensor that can localize in two dimensions the position of touch (Fig. 6.17(c)). In practice, we use the ADC board plugged into a PC to acquire the signal from all the fibers and the touch position can then be monitored on the computer screen via custom LabVIEW software.

6.5.2 Cross-talk and channel calibration

Finally, we address the question of cross-talk between the fibers in the woven 2-D touch pad sensor. As discussed earlier, the sensor comprises a 1-D fiber array separated by 1 cm of textile (Fig. 6.17). In principle, false responses in our system could be induced by cross-talk between individual fibers, which may lead to interference effects between measured signals. In this case, the electrical signal at one channel may induce the signal at the other channel, which might be detected as a false touch. In Fig. 6.18, we show an example of a typical recorded voltage response as a function of time for the three neighboring fibers in the touch pad. No detectable cross-talk between the fibers was observed during recording. Dips on the graphs correspond to the individual touch events that take place at different moments in time. As can be seen in Fig. 6.18, after each touch and release, all the sensor channels successfully return back to the idle state. We notice that fibers in

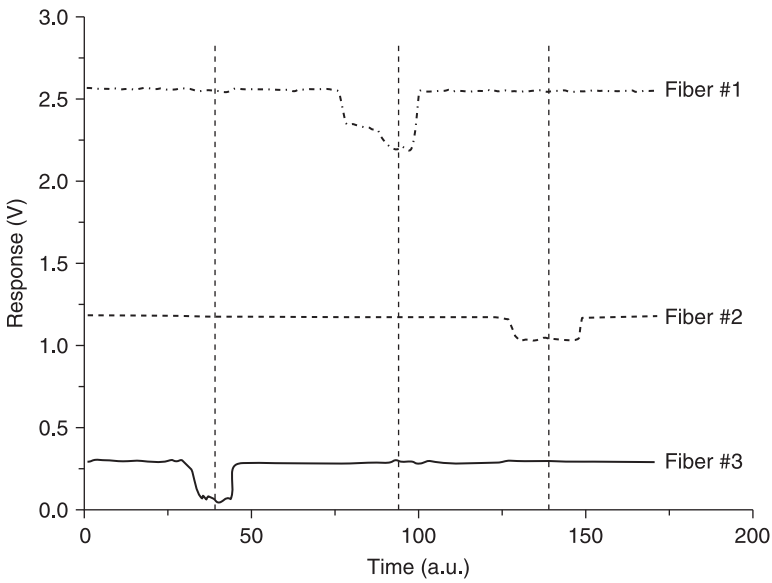

6.18 Recorded voltage response as a function of time for the three neighboring fibers in the woven touch pad. No detectable cross-talk between the fibers was observed. Dips on the graphs correspond to the individual touch events that take place at different moments in time.

Fig. 6.18 have different idle levels, which is explained by all of them having slightly different resistance and capacitance, so the real (not normalized) signal is presented mainly for demonstration purposes. Despite the fact that in the simplest interrogation configuration each individual fiber incorporated into the textile is not multi-touch sensitive (only the closest to the outer electrode touch will be detected), the absence of inter-channel cross-talk enables simultaneous interrogation of the individual slide sensors. In this sense, a 2-D touch pad has a partial multi-touch functionality.

6.6 Conclusion

In conclusion, we have described fabrication, electrical characterization and integration into tactile sensors of the novel all-polymer soft capacitor fibers. The capacitor fibers featuring relatively high capacitance and resistance were fabricated using fiber drawing technique. For ease of connection, a thin copper wire was integrated into the fiber core during the drawing procedure. Soft-capacitor fibers have a typical capacitance per unit length of 69 nF/m, and a typical resistivity parameter of 5 kΩ·m. Our measurements and theoretical modeling show that the fiber capacitance is a very stable, geometry defined parameter independent of the fiber diameter, and fiber fabrication parameters. In contrast, fiber resistivity has a very strong positive temperature coefficient, is highly sensitive to stretching and it is strongly dependent on the fiber drawing parameters.

Next, an individual capacitor fiber was demonstrated to act as a slide sensor that allowed determining the touch position along its length by measuring the fiber AC response at a single point at the fiber surface. Electrical response of such a sensor was described by the RC ladder model, with the modeling data in excellent agreement with experimental observations.

Developed capacitor fibers are soft, small diameter, lightweight and do not use liquid electrolytes, thus they are ideally suited for the integration into textile products. At the end of the chapter, we have demonstrated that by weaving a 1-D array of capacitor fibers (in parallel to each other), a fully woven 2-D touch pad sensor can be built. Performance of a touch pad sensor was then characterized and the absence of the inter-channel crosstalk was confirmed. We also note that a 2-D touch pad has a partial multi-touch functionality.

6.7 References

Alig I, Skipa T, Lellinger D and Pötschke P (2008), 'Destruction and formation of a carbon nanotube network in polymer melts: rheology and conductivity spectroscopy', *Polymer*, 49, 3524–3532.

Baron W, Blair M and Fries-Carr S (2006), 'Airframe structure-integrated capacitor', *US Patent 6981671*.

Beebe D J, Hsieh A S, Denton D D and Radwin R G (1995), 'A silicon force sensor for robotics and medicine', *Sens Actuat A*, 50, 55–65.

Cao Q, Song Y, Liu Z and Zheng Q (2009), 'Influence of annealing on rheological and conductive behaviors of high-density polyethylene/carbon black composites', *J Mater Sci*, 44, 4241–4245.

Cheng L F and Hong Y P (2001), 'Multifiber ceramic capacitor', *J Mater Sci: Mater Electron*, 12, 187–191.

Chu Z, Sarro P M and Middelhoek S (1995), 'Silicon three-axial tactile sensor', *Transducers*, 1, 656.

Cok R S, Bourdelais R R and Kaminsky C J (2004), 'Flexible resistive touch screen', *US Patent 0212599 A1*.

Dahiya R S, Metta G, Valle M and Sandini G, (2010), 'Tactile sensing: from humans to humanoids', *IEEE Trans Rob*, 26, 1–20.

Dalton A B, Collins S, Muñoz E, Razal J M, Ebron V H, *et al.* (2003), 'Super-tough carbon-nanotube fibres', *Nature*, 423, 703.

Dario P and De Rossi D (1985), 'Tactile sensors and the gripping challenge', *IEEE Spectr*, 22, 46–52.

Dietz P and Leigh D (2001), '*DiamondT*ouch: a multiuser touch technology', *Proceedings of UIST, the 14th Annual ACM Symposium on User Interface Software and Technology*, pp. 219–226.

Eltaib M E H and Hewitt J R (2003), 'Tactile sensing technology for minimal access surgery: a review', *Mechatronics*, 13, 1163–1177.

Engel J, Chen J and Liu C (2003), 'Development of polyimide flexible tactile sensor skin', *J Micromech Microeng*, 13, 359–366.

Feng J and Chan C M (2003), 'Effects of strain and temperature on the electrical properties of carbon black-filled alternating copolymer of ethylene-tetrafluoroethylene composites', *Polym Eng Sci*, 43, 1064–1070.

Gao Y, Guo N, Gauvreau B, Rajabian M, Skorobogata O, *et al.* (2006), 'Consecutive solvent evaporation and co-rolling techniques for polymer multilayer hollow fiber preform fabrication', *J Mater Res*, 21, 2246–2254.

Gray B L and Fearing R S (1996), 'A surface micromachined microtactile sensor array', *Proceedings of the IEEE International Conference on Robotics and Automation*, pp. 1–6.

Gu J F, Gorgutsa S and Skorobogatiy M (2010), 'Soft capacitor fibers using conductive polymers for electronic textiles', *Smart Mater Struct*, 19, 115006.

Hoshi T and Shinoda H (2006), 'A sensitive skin based on touch-area-evaluating tactile elements', *Proceedings of the Symposium on Haptic Interfaces for Virtual Environment and Teleoperator Systems*, pp. 89–94.

Kalendra P W and Piazza W J (1994), 'Automatic calibration of a capacitive touch screen used with a fixed element flat screen display panel', *US Patent 5283559*.

Kim K, Lee K R, Kim W H, Park K B, Kim T H, *et al.* (2009), 'Polymer-based flexible tactile sensor up to 32×32 arrays integrated with interconnection terminals', *Sens Actuators A*, 156, 284–291.

Kolesar E S, Dyson C S, Reston R R, Fitch R C, Ford D G and Nelms S D (1996), 'Tactile integrated circuit sensor realized with a piezoelectric polymer', *Proceedings of the 8th IEEE International Conference on Innovative System Silicon*, pp. 372–381.

Lee S, Buxton W and Smith K C (1985), 'A multi-touch three-dimensional touch-sensitive tablet', *Proceedings of the SIGCHI Conference on Human Factors in Computing Systems*, pp. 21–25.

Leineweber M, Pelz G, Schmidt M, Kappert H and Zimmer G (2000), 'New tactile sensor chip with silicone rubber cover', *Sens Actuat A*, 84, 236.

Nakamura S and Sawa G (1998), 'Percolation phenomena and electrical conduction mechanism of carbon black-polyethylene composites', *Proceedings of the International Symposium on Electrical Insulating Materials*, pp. 1–54.

Park C S, Park J and Lee D W (2009), 'A piezoresistive tactile sensor based on carbon fibers and polymer substrates', *Microelectron Eng*, 86, 1250–1253.

Rekimoto J, *et al.* (2002), 'SmartSkin: An infrastructure for freehand manipulation on interactive surfaces', *Proceedings of the SIGCHI Conference on Human Factors in Computing Systems*, pp. 113–120.

Ruspini D C, Kolarov K and Khatib O (1997), 'Proceedings of the symposium on haptic interfaces for virtual environment and teleoperator systems', *Proceedings of the 24th Annual Conference on Computer Graphics and Interactive Techniques*, pp. 345–352.

Schulte B, Tischer W, Waldenrath W and Kaloff H (1988), 'Stretched polycarbonate films filled with carbon black', *US Patent 4791016*.

Shimojo M, Namiki A, Ishikawa M and Makino R (2004), 'A tactile sensor sheet using pressure conductive rubber with electrical-wires stitched method', *IEEE Sens J*, 4, 589–595.

Tang H, Chen X and Luo Y (1997), 'Studies on the PTC/NTC effect of carbon black filled low density polyethylene composites', *Eur Polym J*, 33, 1383–1386.

Wolffenbuttel M R and Regtien R P L (1991), 'Polysilicon bridges for the realization of tactile sensors', *Sens Actuat A*, 26, 257–264.

Wu G, Asai S, Zhang C, Miura T and Sumita M (2000), 'A delay of percolation time in carbon-black-filled conductive polymer composites', *J Appl Phys*, 88, 1480–1487.

Yu G, Zhang M Q and Zeng H M (1998), 'Carbon-black-filled polyolefine as a positive temperature coefficient material: effect of composition, processing, and filler treatment', *J Appl Polym Sci*, 70, 559–566.

Yuji J and Sonoda C (2006), 'PVDF tactile sensor for static contact force and contact temperature', *Proc IEEE Sens*, 738–741.

Zhang W, Dehghani-Sanij A A and Blackburn R S (2007), 'Carbon based conductive polymer composites', *J Mater Sci*, 42, 3408–3418.